*Progress in Photovoltaics: Research and Applications*

WILEY

PROGRESS IN PHOTOVOLTAICS

RESEARCH ARTICLE

# Understanding ERE and $iV_{OC}$ Metrics for Graded CdSeTe Absorbers

Dmitry Krasikov[1] | Darius Kuciauskas[2] | Patrik Ščajev[3] | Rouin Farshchi[4] | Kevin McReynolds[1] | Igor Sankin[1]

[1]Advanced Research, First Solar, Perrysburg, Ohio, USA | [2]Chemistry and Nanoscience Center, National Renewable Energy Laboratory, Golden, Colorado, USA | [3]Institute of Photonics and Nanotechnology, Faculty of Physics, Vilnius University, Vilnius, Lithuania | [4]California Technology Center, First Solar, Santa Clara, California, USA

**Correspondence:** Dmitry Krasikov (dmitry.krasikov@firstsolar.com)

**Received:** 13 September 2024 | **Revised:** 14 February 2025 | **Accepted:** 22 April 2025

**Keywords:** CdTe | ERE | $iV_{oc}$ | mobility | modeling | photoluminescence | quasi-Fermi level

## ABSTRACT

PL-based external radiative efficiency (ERE) and implied open-circuit voltage ($iV_{OC}$) metrics were introduced for thin-film solar absorbers to better understand the voltage deficit and diagnose losses in solar cells. Traditionally, elevated ERE and $iV_{OC}$ measurements are associated with diminished recombination within the solar device, a rationale heavily reliant on the assumption of a uniform bandgap and high carrier mobilities in the absorber. Recently, very low mobilities in CdSeTe absorbers ($< 1\,cm^2/(V{\cdot}s)$) were measured using the light-induced transient grading technique. In this study, we use a detailed numerical model of $iV_{OC}$ to investigate the possible reasons of elevated $iV_{OC}$ in realistic CdSeTe absorbers with a graded Se profile. In particular, we examine how the bandgap nonuniformity and the reduced hole mobility in graded CdSeTe absorbers affect $iV_{OC}$ measurements. We show that high $iV_{OC}$ may result from inflated quasi-Fermi level splitting in the high-Se region in the front part of a CdSeTe absorber with slow hole transport. We reproduce the experimentally reported 360 mV increase in $iV_{OC}$–$V_{OC}$ gap with reduced doping using a model with sub-1 $cm^2/(V{\cdot}s)$ hole mobility in the high-Se region. Based on our results, we conclude that the $iV_{OC}$ metric (or ERE metric) should not be used as a sole metric of CdSeTe absorber quality. We discuss possible ways to extract useful information from the $iV_{OC}$–$V_{OC}$ gap by supplementing the front-side illumination measurements with back-side illumination measurements.

## 1 | Introduction

Even though thin-film solar cells with CdSeTe absorbers recently achieved a record-breaking 23.1% efficiency [1], they still have not reached their full potential. One way to realize this potential is to understand where and why losses occur in a device, e.g., absorber vs. contacts, and address these issues separately by adjusting process parameters. However, diagnosing device losses is not a straightforward task in complex devices such as CdSeTe cells. CdSeTe cells have an absorber with a graded Se composition (Se% = Se / (Se + Te)), ranging from 20%–30% at the front to 0%–5% at the back, with various material properties depending on the Se%. In addition, the absorber has two interfaces (front and back), which potentially contribute to recombination and constitute carrier extraction barriers. Certain indirect characterization techniques may not be directly applicable to CdSeTe or may require very involved interpretation and additional modeling to be properly understood.

Photoluminescence (PL) measurements are widely used for solar cell characterization. It is agreed that a high efficiency cell has bright PL [2] and a high PL-based external radiative efficiency (ERE) [3, 4] metric. Achieving bright PL from a solar cell is often set as a goal because it should signify reduced nonradiative recombination, which is true when the quasi-Fermi level splitting (QFLS) is uniform throughout the absorber [5, 6]. For QFLS to be uniform, the carrier mobilities must be high enough that the electron/hole quasi-Fermi levels, $QFL_{n/p}$, are "equilibrated"

(flat) throughout the absorber. This may not always be the case, especially for realistic CdSeTe cells with limited carrier mobilities. There has been no comprehensive study on the relationship between PL and the properties of solar cell absorbers with nonuniform QFLS.

To assess the absorber quality and partition the losses between the absorber and interfaces, an additional PL-based metric, implied open-circuit voltage ($iV_{OC}$), was introduced [7–9]. $iV_{OC}$ is intended to measure QFLS in the absorber and is defined as $V_{OC,ideal} + kT{\cdot}\log$ (ERE), where $V_{OC,ideal}$ is the $V_{OC}$ with radiative recombination only. It requires two contactless measurements: the absolute PL to calculate ERE and the absorptance spectrum to calculate $V_{OC,ideal}$ [7]. Originally, the $iV_{OC}$ method was introduced for an absorber with a uniform $E_g$ and uniform QFLS [5]. Such an absorber has uniform carrier densities, uniform radiative recombination rates, and high mobilities. Later, based on a combination of simulations and experiments, three different scenarios of $QFL_{n/p}$ bending were recognized to lead to a QFLS/q–$V_{OC}$ gap, i.e., QFL bending near the corresponding contact, majority QFL bending inside the absorber, and majority QFL bending inside the contact (Figure 1) [10–18].

In the first scenario, the QFLS/q–$V_{OC}$ gap appears due to $QFL_{n/p}$ bending in the absorber near the recombinative interface with the *n*- or *p*-contact [10–12]. This is depicted schematically in Figure 1A,B, where $QFLS_{MAX}$ denotes the maximum QFLS. $QFL_{n/p}$ bending is caused by low n/p mobility in the absorber, leading to incomplete $QFL_{n/p}$ "equilibration" between the absorber and the corresponding contact.

In the second scenario, the QFLS/q–$V_{OC}$ gap is caused by QFLS reduction from front to back due to bending of the majority QFL (Figure 1C) [13–15]. This QFL bending occurs when the mobility of the majority carrier is not high enough to fully "equilibrate" the QFL between the high-generation region near the front and the rest of the absorber. We note that QFLS reduction from front to back due to bending of the minority QFL is also possible, but it does not cause a QFLS/q–$V_{OC}$ gap and is not important in the context of this paper.

The last scenario is $QFL_{n/p}$ loss inside the *n*/*p*-contact (Figure 1D). This happens when the *n*/*p*-contact resistivity is too high and when the work function of the electrode connected to the *n*/*p*-contact layer is too high/low [16, 17]. This scenario leads to very low $J_{SC}$ and near-zero efficiency [16] and does not occur in realistic working solar cells.

Because $iV_{OC}$ is not a direct measurement of QFLS and QFLS may be nonuniform, it is not always clear what the $iV_{OC}$ metric means and how it relates to QFLS. In addition to QFLS nonuniformity, other factors may affect the PL-based $iV_{OC}$ metric, such as nonuniform radiative recombination through the absorber due to nonuniform $E_g$, incomplete internal PL reflection from the back interface (BI), and emission from radiative defects.

What about the ERE and $iV_{OC}$ measurements in realistic CdSeTe absorbers? For record-efficiency CdSeTe devices ($V_{OC} = 900$ mV), $iV_{OC} \leq 920$ mV (ERE ≤ 0.1%) [19]. A much higher $iV_{OC}$ of 970 mV (ERE ≈ 1%–2%) was reported [7] for an As-doped graded CdSeTe cell from Colorado State University.

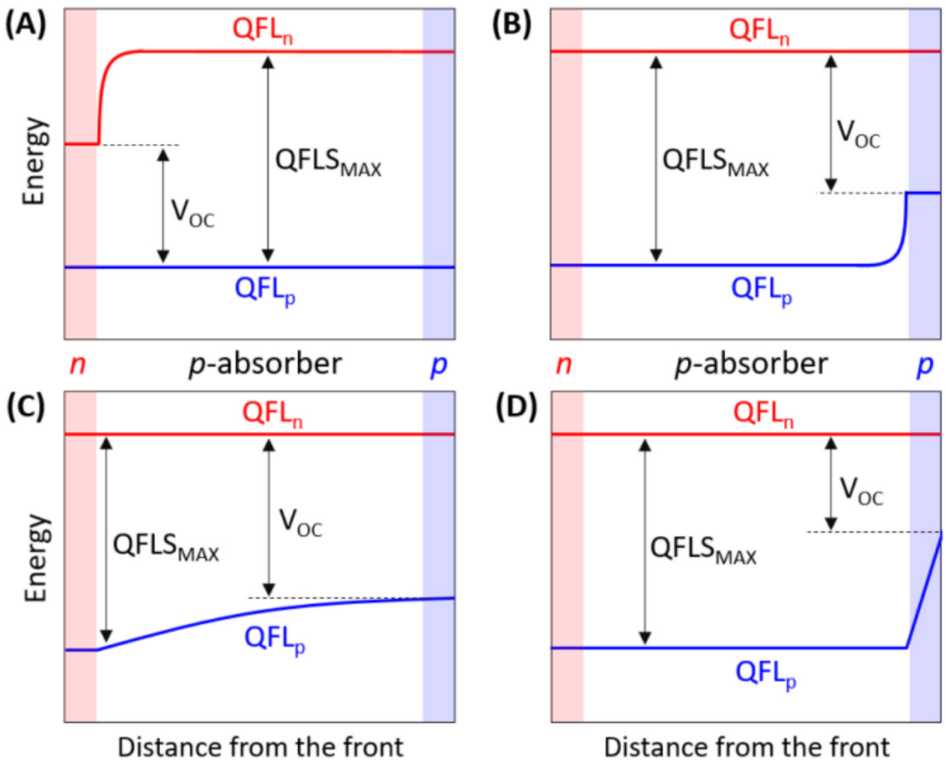


**FIGURE 1** | Schematic of different scenarios resulting in a QFLS/q–$V_{OC}$ gap: (A) $QFL_n$ bending near the *n*-contact, (B) $QFL_p$ bending near the *p*-contact, (C) majority carrier QFL bending inside the absorber, and (D) $QFL_{n/p}$ loss inside the *n*/*p*-contact.

For As-doped cells with good contacts, the authors of Ref. [7] report increased $iV_{OC}$ and larger $iV_{OC}$–$V_{OC}$ gap with lower absorber doping. In all cases, the authors interpret higher ERE and $iV_{OC}$ as a signature of better absorber. In this paper, we provide an alternative explanation for increased $iV_{OC}$ in CdSeTe absorbers with low hole mobility using detailed $iV_{OC}$ modeling.

The high carrier mobility values reported for single-crystal CdTe ($\mu_n \sim 1000\,cm^2/(V{\cdot}s)$, $\mu_p \sim 80\,cm^2/(V{\cdot}s)$) [20] might not be representative of the properties of the typical thin-film polycrystalline CdTe absorbers. Additionally, in alloys, mobilities may be lower than in the corresponding binary materials [21, 22]. So far, we have only discussed the effect of mobilities on "equilibration" of the $QFL_{n/p}$. Solar cell physics suggests that it is in fact the product of mobility and carrier density (i.e., partial conductivity) that defines currents of carrier and affects carrier separation efficiency [23]. The net *p*-doping (difference between acceptors and donors) as measured by CV can reach $10^{16}\,cm^{-3}$ in As-doped CdSeTe cells. At the same time, the free hole density can be lower when the acceptors are nonshallow and the doping is compensated [24, 25]. This is exactly the case for CdTe and CdSeTe absorbers [19, 26–28]. Furthermore, increased Se content in CdSeTe deteriorates *p*-dopability [26, 29, 30] and causes the ionization levels of acceptors to become deeper compared to pure CdTe [31, 26, 27], which may reduce the hole density in the high-Se region of a graded absorber. If the hole mobility also becomes low in the high-Se region, this may result in very low hole partial conductivity, affecting $QFL_p$ equilibration.

In this paper, we explain the meaning of high $iV_{OC}$ values in graded CdSeTe absorbers by using previously measured low carrier mobilities with numerical drift–diffusion simulations of $iV_{OC}$. In Section 2, we describe device model and $iV_{OC}$ model, validation of $iV_{OC}$ model, and the range of mobilities obtained from experimental measurements. In Section 3, we analyze the effect of nonuniform $E_g$ and nonuniform QFLS on $iV_{OC}$. We investigate the different scenarios of nonuniform QFLS described in Figure 1A–C and conclude that an $iV_{OC}$–$V_{OC}$ gap above a certain threshold indicates QFLS nonuniformity due to carrier transport issues. We simulate the experimentally reported effect of doping activation on the $iV_{OC}$–$V_{OC}$ gap. To distinguish between different scenarios for the QFLS/q–$V_{OC}$ gap, we provide practical recommendations based on $iV_{OC}$–$V_{OC}$ gap measurement with front- and back-side illumination. In Section 4, we discuss the physical meaning of $iV_{OC}$ and selectivity metrics, the remaining sources of $iV_{OC}$ error, and how our modeling results affect the interpretation of experimental $iV_{OC}$ data. Section 5 provides a brief summary of the most important conclusions.

## 2 | Numerical Experiment and Parameters

In this section, we describe a CdSeTe cell stack, a numerical model for $iV_{OC}$, validation of this model on a simple device structure, and experimental measurements of hole mobility that allow us to narrow the range of carrier mobility values used in simulations.

### 2.1 | CdSeTe Cell Stack

The solar cell stack used in simulations consists of an $n^+$-type front contact layer at the front, *n*-type buffer, a 3-μm *p*-type absorber (with uniform or graded $E_g$), and a $p^+$-type contact at the back (Figure 2). The front interface (FI) has a valence band offset (VBO), and the BI has conduction band offset (CBO), preventing the minority carrier from entering the corresponding contact layer (electrons cannot enter $p^+$-contact; holes cannot enter $n^+$-contact).

In this work, we define "contacts" as being coincidental with the $n^+$-contact and buffer at the front and $p^+$-contact layer at the back and as being able to conduct only one type of free carrier. We define "absorber" as being fully coincidental with the physical absorber layer, even though photogeneration can be very low in the low-Se region near the back of a graded CdSeTe absorber. This is opposed to the conceptual definitions in Ref. [16], where the absorber is defined as the high-generation region only, and the contacts can include some part of the absorber layer and conduct both types of carriers.

### 2.2 | Numerical Model for $iV_{OC}$

To calculate ERE and $iV_{OC}$, we first need to find the device steady-state by solving the drift–diffusion + reaction equations for electrons and holes and the Poisson equation for charge conservation (see, e.g., Refs. [32, 33], or Section 5.7 in Ref. [34]). To calculate $V_{OC}$, we apply 1 sun AM1.5G irradiance and find the steady-state solution with the total current through the cell equal to zero. QFLS is calculated as the difference between the electron and hole QFL in the absorber.

For all calculations, we use our internally developed numerical solver, E-Solver. All physics in E-Solver, i.e., the underlying equations, definition of solar cell stack layers, photogeneration, defects, recombination, interface states, and band offsets, are fully consistent with SCAPS 1D solar simulator [35]. To verify E-Solver solutions, we performed a number of benchmarking tests paying special attention to the test cases with low electron or hole mobility. Figures S1 and S2 show

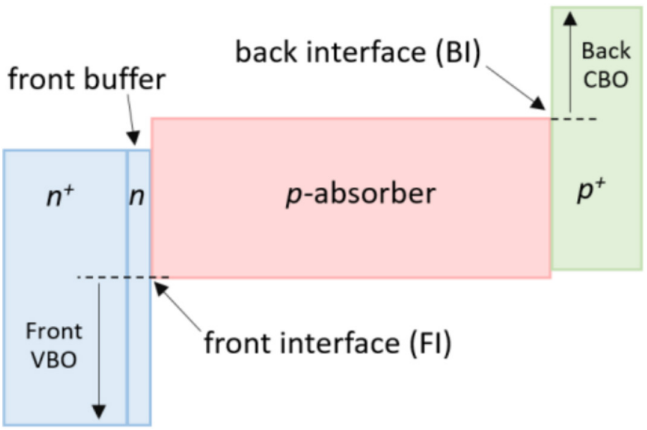


**FIGURE 2** | Schematic of the $n^+/n/p/p^+$ solar cell stack used in simulations.

that E-Solver accurately reproduces SCAPS 1D band diagrams for uniform absorbers with low electron/hole mobilities, including the $QFL_{n/p}$ bending. Tests with different electron/hole mobilities show that the QFLS/q–$V_{OC}$ difference from E-Solver tracks the one from SCAPS with an error of ≤ 2 mV in most cases (Figures S1A and S2A). Two SCAPS 2D definition files for the problems with low electron/hole mobilities can be found in Supporting Information. More details on E-Solver will be published elsewhere.

After the steady-state solution is obtained, we calculate $iV_{OC}$ as proposed in the literature [7]:

$$iV_{OC} = V_{OC,ideal} + kTlog(ERE) \quad (1)$$

$V_{OC,ideal}$ is $V_{OC}$ of an ideal device, which is limited by radiative recombination only and does not have any carrier extraction issues. To calculate $V_{OC,ideal}$ in E-Solver, we use very high mobilities and nonradiative lifetimes and very low recombination rates at the FI and BI. The position-dependent radiative recombination rate is calculated using the position-dependent absorption spectrum.

ERE is calculated as

$$ERE = \Phi_{PL} / \Phi_{exc} \quad (2)$$

$\Phi_{PL}$ is the outcoming steady-state PL photon flux obtained by integrating the spatially- and energy-resolved radiative recombination flux in the absorber under open-circuit conditions taking into account reabsorption and reflection from the FI/BI of the absorber [34]

$$\Phi_{PL} = \int_{E=0}^{\infty}\int_{x=0}^{d} R\frac{\alpha(E,x)\cdot(E)^2}{2\pi^2\hbar^3c_0^2 e^{\frac{(E-QFLS(x))}{kT}}-1}dxdE$$
$$R = (1-R_{FC})\left\{e^{-\alpha(E,x)x} + R_{BC}e^{-\alpha(E,x)(2d-x)}\right\} \quad (3)$$

The term after $R$ describes the flux that is able to escape the device (inside the emission cone), which is lower than the total internal photon flux. $\alpha(E,x)$ is the position-dependent absorption spectrum of CdSeTe, $E$ is the photon energy, and $x$ is the distance from the front contact. The term $R$ describes the fraction of emission that does not escape through the back side and is not reabsorbed in the absorber, where $d$ is the absorber thickness, $R_{FC}$ is the internal reflectance of the front contact, and $R_{BC}$ is the internal reflectance of the back contact. We consider all reabsorbed PL as lost, because in all realistic CdSeTe cells, the radiative efficiency is < 1%; hence, the re-emission probability is very low.

The excitation photon flux, $\Phi_{exc}$, is calculated by integrating the spatially- and energy-resolved photogeneration rate:

$$\Phi_{exc} = \int_{E=0}^{\infty}\int_{x=0}^{d}\Phi_{1sun}(E)\cdot e^{-\alpha(E,x)\cdot x}dxdE \quad (4)$$

where $\Phi_{1sun}(E)$ is the energy-resolved solar photon flux.

## 2.3 | Validation of $iV_{OC}$ Model

To validate our $iV_{OC}$ model, we simulate uniform CdTe absorber with different lifetimes in the limit of very high mobilities ($\mu_n = \mu_p = 10^6\,cm^2/(V\cdot s)$). In this case, the $QFL_{n/p}$ is always flat, and QFLS is uniform. The model includes 100% internal reflectance from the back contact and 100% transmittance of the front contact. The calculated difference between $iV_{OC}$ and QFLS/q is small over the entire range of lifetimes (Figure 3A). We verified that the result is weakly dependent on the number of mesh points (Figure 3A compares a coarse 200-point mesh with a fine 1000-point mesh for doping = $10^{15}\,cm^{-3}$). We also compare different doping levels ($10^{15}$–$10^{16}\,cm^{-3}$) and different doping models. Most of the calculations use simple uncompensated doping with shallow acceptors where [doping] = [Acceptors] = $p$. We also use a more realistic model of compensated doping with nonshallow acceptors, where $p$ < [doping]: the concentration of donors is $10^{18}\,cm^{-3}$, and the concentration of acceptors is $1.01\cdot10^{18}\,cm^{-3}$, so that the net doping is $10^{16}\,cm^{-3}$ and the doping activation ratio is 1%. The acceptor ionization level is 0.13 (0.16 eV) in CdTe ($CdSe_{0.25}Te_{0.75}$), which corresponds to our calculated $As_{Te}$ ionization levels [36]. Since the calculated $iV_{OC}$–QFLS/q difference is less than 0.5 mV in all cases, we conclude that the $iV_{oc}$ model is correct.

## 2.4 | Electron and Hole Mobility Ranges for the Simulations

To determine the range of carrier mobility values to use in numerical simulations, we use the carrier mobilities for heterostructures with uniform $CdSe_xTe_{1-x}$ absorber as well as with graded CdSeTe absorber recently published in Ref. [37]. The hole effective mass in CdTe is considerably higher than that of electrons; therefore, hole mobilities can be estimated as half of the ambipolar mobilities measured in Ref. [37]. As Se% increases from 0% to 40% in a uniform absorber, the hole mobility at picosecond timescales decreases from ~20 to 5 $cm^2/(V\cdot s)$ (~2.5 $cm^2/(V\cdot s)$ with a high As concentration). The hole mobilities at nanosecond timescales are lower (< 1 ns in all cases), which is explained by carrier trapping on longer time scales. The lowest measured values of nanosecond-timescale hole mobility are ~0.1 $cm^2/(V\cdot s)$. The highest values of picosecond-timescale hole mobility measured from the low-Se side of graded absorbers are ~35 $cm^2/(V\cdot s)$. Since the relationship between these nanosecond- and picosecond-timescale mobilities and steady-state mobilities is not immediately clear, we use the range 0.1–100 $cm^2/(V\cdot s)$ for hole mobility and 1–1000 $cm^2/(V\cdot s)$ for electron mobility.

# 3 | $iV_{OC}$ Modeling Results

In this section, we present our study of the effect of absorber grading and illumination direction on $iV_{OC}$ using the $iV_{OC}$ model described in the previous section. Generally, two quantities may be nonuniform in a graded CdSeTe absorber: $E_g$ and $QFL_{n/p}$. We analyze the effect of $E_g$ nonuniformity in Section 3.1 and the effect of $QFL_{n/p}$ nonuniformity in Section 3.2. Section 3.3 describes the effect of reduced doping activation on increased $iV_{OC}$-$V_{OC}$ gap. Section 3.4 describes $iV_{OC}$ modeling results with back-side illumination and the

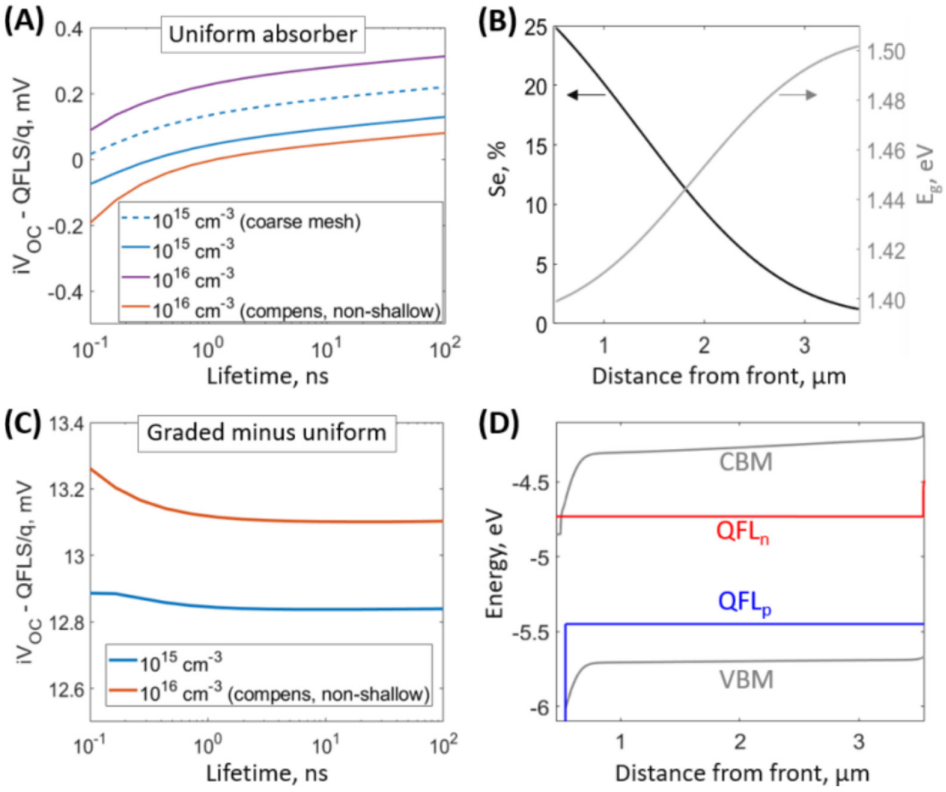


**FIGURE 3** | (A) Calculated $iV_{OC}$–QFLS/q difference for different lifetimes and absorber doping models. For doping = $10^{15}\,cm^{-3}$, a comparison of coarse mesh (200 mesh points) with fine mesh (1000 points) shown. For doping = $10^{16}\,cm^{-3}$, a comparison of simple uncompensated doping model with compensated doping with nonshallow acceptors shown. (B) Se%(x) and $E_g$(x) profiles in graded CdSeTe absorber used in simulations. (C) Calculated $iV_{OC}$–QFLS/q difference for graded absorber relative to $iV_{OC}$–QFLS/q difference for the uniform absorber shown in (A). (D) Band diagram for graded absorber with $\mu_n = \mu_p = 10^6\,cm^2/(V{\cdot}s)$ at open-circuit condition (1 sun).

possible use of back-side $iV_{OC}$–$V_{OC}$ gap measurement in understanding of QFLS/q–$V_{OC}$ gap in the device.

### 3.1 | Graded Absorber: Effect of $E_g$ Grading

In order to analyze the effect of $E_g$ on $iV_{OC}$, we simulate $iV_{OC}$ in the limit of very high mobilities ($\mu_n = \mu_p = 10^6\,cm^2/(V{\cdot}s)$) with a nonuniform Se profile in the CdSeTe absorber. The Se% changes from 25% at the FI to 2% at the BI (Figure 3B). Using $E_g$ (Se%) bandgap bowing [38], we set a nonuniform $E_g$ distribution in the absorber, $E_g$(x), (Figure 3B), and a nonuniform absorption spectrum, obtained by shifting the CdTe absorption spectrum according to $E_g$(x) (see Figure S3). A $V_{OC,ideal}$ value of 1.147 V is calculated as the $V_{OC}$ of a device with radiative recombination only (as described in Section 2.2).

By doing a series of calculations with different lifetimes in the absorber, we find that the $iV_{OC}$–QFLS/q gap exceeds that in the uniform absorber by approximately 13 mV (Figure 3C). In the limit of high mobilities, QFLS remains uniform in the graded absorber, because electrons and holes are fast enough to "equilibrate" (flatten) the $QFL_{n/p}$ (Figure 3D). To understand the reason for the 13mV overestimation, we analyze how PL reabsorption in a graded absorber is different from that in a uniform absorber.

In a uniform absorber, radiative recombination occurs uniformly throughout the absorber, and the PL emitted from the rear part of the absorber experiences significant loss due to reabsorption before it leaves the device. The simple expression for $iV_{OC}$ (Equation 1) was derived specifically for this scenario [5] and allows for correct $iV_{OC}$ prediction for a uniform absorber.

In a graded absorber, the radiative emission rate is dominated by the front region of the absorber where $E_g$ is lower (~1.4 eV) than at the back of the absorber (~1.5 eV). Since the emission mostly comes from the front, it experiences less reabsorption, and the outcoming PL is brighter than the PL from a uniform absorber with the same QFLS. Since the expression for $iV_{OC}$ (Equation 1) assumes that the absorber is uniform, it predicts $iV_{oc}$ assuming stronger PL reabsorption, and it ascribes brighter PL from a graded absorber to a larger QFLS rather than to lower reabsorption.

This is why, in the limit of high mobilities, the simple $iV_{OC}$ expression overestimates QFLS/q by ~13 mV for a 3 μm graded absorber with the Se profile shown in Figure 3B. For 2 and 4 μm graded absorbers, $iV_{OC}$ overestimates the QFLS/q by approximately 16 and 10 mV, respectively. We expect that these numbers would vary slightly with different Se profiles.

### 3.2 | Graded Absorber: Effect of Low Mobilities

Here, we analyze the effect of nonuniform $QFL_{n/p}$ on the $iV_{OC}$ metric. Instead of artificially high carrier mobilities used in

Section 3.1, we now use more realistic mobilities, so that, in addition to nonuniform $E_g$, the $QFL_{n/p}$ may also become nonuniform. Here, we consider device models relevant to high-efficiency cells with an As-doped graded CdSeTe absorber. We use two constraints: net doping = $10^{16}$ $cm^{-3}$ (difference between acceptor and donor concentration) and high performance metrics ($V_{OC}$ > 850 meV, FF > 75%, and $J_{sc}$ > 31 mA/$cm^2$). Using the $iV_{OC}$ model, we investigate possible reasons for $iV_{OC} > V_{OC}$ in such devices with nonuniform $E_g$ and $QFL_{n/p}$. For now, we only consider $V_{OC}$ and $iV_{OC}$ metrics calculated with front-side illumination.

With realistic mobilities ($\mu_p$ = 0.1–20 $cm^2$/(V·s), $\mu_n \sim 10\times$ higher than $\mu_p$), the $QFL_{n/p}$ may vary throughout the absorber or just in the vicinity of one contact. Calculations show that $iV_{OC}$ qualitatively follows $QFLS_{MAX}$; however, it may be higher or lower than $QLFS_{MAX}$, depending on the model parameters. When $iV_{OC} - V_{OC} > 13$ mV (3-μm absorber), this means $QFLS_{MAX}/q > V_{OC}$, i.e., there is large QFLS somewhere in the absorber, and there is QFLS loss that reduces device $V_{OC}$. All such models can be grouped into three categories (similar to scenarios in Figure 1A–C): (i) $QFL_n$ bending near the *n*-contact, (ii) $QFL_p$ bending near the *p*-contact, and (iii) $QFL_p$ bending inside the absorber. Below, we consider these three categories in detail.

**(i) $QFL_n$ bending near the *n*-contact**. With strong FI recombination and low $\mu_n$ near the front, photogenerated electrons may be "out of equilibrium" with the front contact electrons leading to $QFL_n$ bending near the FI (Figure 4A). As a result, QFLS reduces toward the FI, giving $V_{OC} < QFLS_{MAX}/q$. Strong FI recombination requires a negative CBO (cliff) at the FI and FI recombination centers. A cliff CBO reduces the interface $E_g$ (defined as *n*-contact CBM–absorber VBM) and allows more holes to reach the FI to participate in recombination [39]. According to atomistic modeling, a cliff CBO may form at the CdTe/$SnO_2$ interface in the case of incomplete passivation by Cl [40].

Figure 4D shows that with decreasing electron mobility, both the QFLS/q–$V_{OC}$ gap and $iV_{OC}$–$V_{OC}$ gap increase. A significant $iV_{OC}$–$V_{OC}$ gap requires very low electron mobility (< 10 $cm^2$/(V·s)), which may not be realistic. However, based on our calculations, the $iV_{OC}$–$V_{OC}$ gap can be pronounced even with $\mu_n$ > 100 $cm^2$/(V·s) if cliff CBO and FI acceptor lead to electron depletion near the FI (not shown in Figure 4). This may occur when a large density of acceptor defects forms at or near the FI, as suggested by 1D kinetic simulations of *p*-doping formation in *n*-TCO/absorber stacks [26].

**(ii) $QFL_p$ bending near the *p*-contact**. With strong recombination at the BI and low $\mu_p$ at the back of the absorber (i.e., in the low-Se region), photogenerated holes may be "out of equilibrium" with the back contact, leading to $QFL_p$ bending near the BI (Figure 4B). This reduces QFLS near the BI, resulting in $V_{OC} < QFLS_{MAX}/q$. This requires strong BI interface recombination, which is caused by a combination of BI VBO and BI recombination centers. A relatively small VBO of 0.03 eV was suggested based on calculations with isolated CdTe and ZnTe slabs [41]. Alloying CdTe with Se may further increase the valence band offset because the CdSeTe VBM is lower than that of CdTe [40]. Larger VBO could be expected due to the interface dipolar term when the materials are brought into contact [42].

Similar to the case with FI recombination, a lower $\mu_p$ at the back of the absorber increases the QFLS/q–$V_{OC}$ gap and $iV_{OC}$–$V_{OC}$

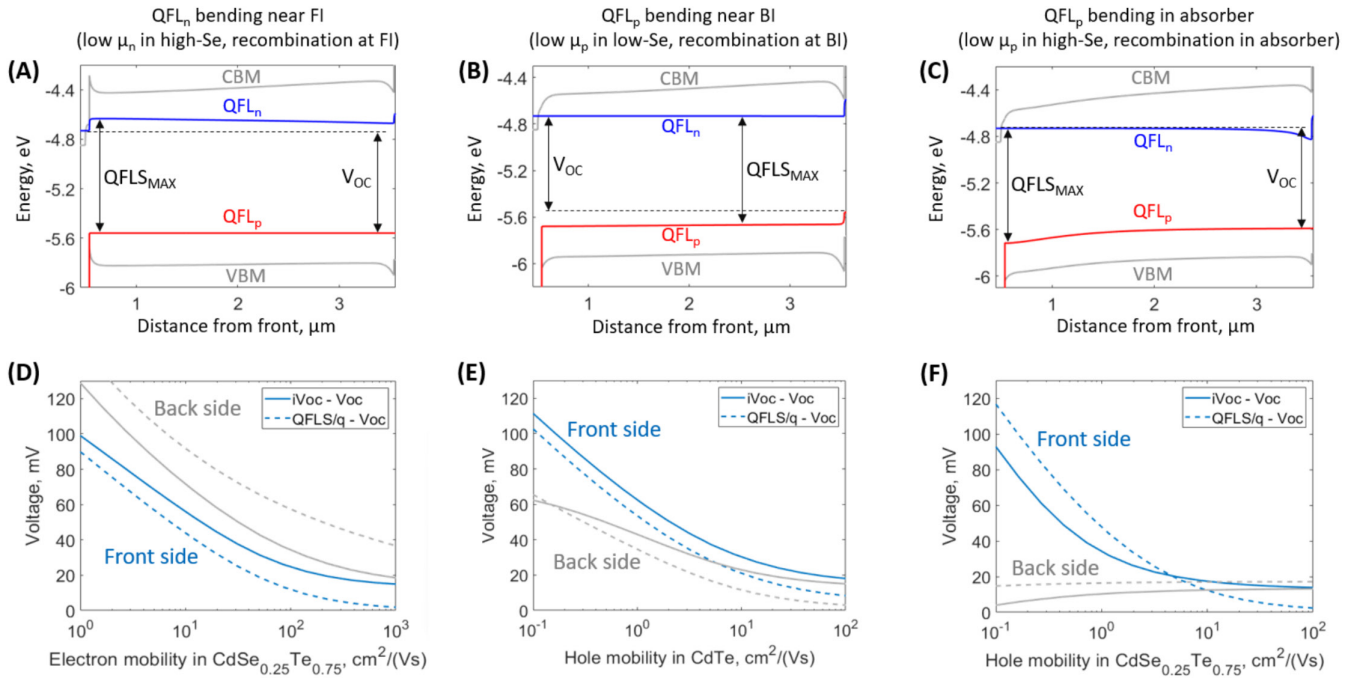


**FIGURE 4** | (A)–(C) band diagrams and (D)–(F) dependence of QFLS/q–$V_{OC}$ gap on carrier mobility for three cases with $QFL_n$ bending near the FI (A, D), near the BI (B, E) and inside the absorber (C, F). Panels (D)–(F) compare the $iV_{OC}$–$V_{OC}$ gap with the QFLS/q–$V_{OC}$ gap for two different illumination directions: "front side," simulated with illumination through the $n^+$-TCO, and "back side," simulated with illumination through the $p^+$-ZnTe. All model parameters can be found in Tables S1 and S2.

gap (Figure 4E). Theoretically, a QFLS/q–$V_{OC}$ gap may appear in real high-efficiency devices due to $QFL_p$ bending near the *p*-contact. However, this requires strong BI recombination, meaning that the BI quality is low (large band offset and defects). At the same time, the quality of the FI and absorber should be sufficient to allow photogenerated electrons to reach the BI without recombining.

In both cases (FI and BI recombination), the $iV_{OC}$ metric is consistently higher than QFLS/q by 10–15 mV (Figure 4D,E), but the exact value of the QFLS/q–$V_{OC}$ gap depends on the doping model and on the recombination parameters.

**(iii) $QFL_p$ bending inside the absorber.** When the hole mobility in the high-Se region of the absorber is low, holes in the high-photogeneration region at the front may be "out of equilibrium" with the holes in the rest of the absorber. The $QFL_p$ becomes nonuniform, and the QFLS decreases through the absorber from front to back, leading to $V_{OC}$ < QFLS/q (Figure 4C). The outcoming PL photon flux increases because the larger QFLS near front leads to a higher radiative recombination rate. In addition, PL generated closer to the front experiences less reabsorption. As a result, both ERE and $iV_{OC}$ increase (Figure 4F). A 10× increase in ERE results in an ~60 mV increase in $iV_{OC}$. Importantly, the lifetime remains the same in all simulations, so the $iV_{OC}$ increase is not the result of a higher lifetime. Moreover, simulations suggest that a higher $iV_{OC}$ may be obtained in an absorber with a lower lifetime if the hole conductivity is reduced.

Theoretically, the three scenarios discussed above provide a comprehensive list of potential cases with overestimated $iV_{oc}$ for CdSeTe cells with reasonably high efficiency. The only remaining case is $QFL_n$ bending in the rear region of the absorber or near the back contact. However, such $QFL_n$ bending does not increase the $iV_{OC}$–$V_{oc}$ difference and therefore, is excluded from our consideration. Among the three scenarios considered, case (iii) "$QFL_p$ bending inside the absorber" is the most realistic. It does not require excessively low electron mobility, and the hole mobility is graded with the lowest values in high-Se region corresponding to the lower boundary of the measured nanosecond-scale hole mobility.

All model parameters used to generate the results shown in Figure 4A–F are presented in Tables S1 and S2.

We note that the three scenarios of QFL bending above are not exclusive to graded absorbers and can be observed in uniform absorbers under certain conditions. All cases of QFL bending in Figure 4A–C can be simulated with a uniform absorber both in E-Solver and SCAPS 1D simulator (e.g., using SCAPS definition files provided in the Supporting Information), and qualitatively the same conclusions will be reached. In Ref. [18], for example, all three cases were simulated for a uniform CdTe absorber using SCAPS, and the same conclusions regarding the effect of mobilities and doping were obtained. The addition of absorber grading does not qualitatively change any of the conclusions; it only shows how these effects can be reproduced in realistic high-efficiency cells. The main distinctions of the results in Figure 4 compared to what can be simulated in SCAPS are (i) a graded acceptor ionization level (0.13 eV in pure CdTe, 0.16 eV in $CdSe_{0.25}Te_{0.75}$), (ii) a model of PL reabsorption to calculate the outcoming photon flux and ERE, and (iii) a graded radiative recombination rate constant (calculated from the Se-dependent absorption spectrum) used to calculate $V_{OC,ideal}$ and further $iV_{OC}$.

### 3.3 | The Effect of Low Doping Activation

As discussed in Section 1, the hole current is proportional to the partial hole conductivity. Consequently, when the hole mobility or hole density decreases, the $QFL_p$ bending in the absorber can be amplified. The lower the hole mobility and doping activation ratio, the larger the QFLS/q–$V_{OC}$ gap becomes, due to the increased $QFL_p$ bending resulting from the reduced partial conductivity of holes (see Figure S4A,B).

An activation ratio of ~1%–2% is typical for high-efficiency As-doped cells [19], where the CV doping is ~$10^{16}$ $cm^{-3}$, and the total As concentration is 5·$10^{17}$–$10^{18}$ $cm^{-3}$. To understand the effect of a reduced doping activation ratio on the $iV_{OC}$ of a realistic As-doped cell, we calculate $iV_{OC}$ using a model that has recombination in all three main regions: absorber, FI, and BI. For a baseline model, we use a total acceptor density of $10^{18}$ $cm^{-3}$ and a graded hole mobility which varies from 0.3 $cm^2/(V{\cdot}s)$ in $CdSe_{0.25}Te_{0.75}$ to 20 $cm^2/(V{\cdot}s)$ in CdTe (see Table S3 for all parameters of our baseline device model).

When the doping activation ratio reduces from 2% down to 0.005% (net *p*-doping reduces from 2·$10^{16}$ to 5·$10^{13}$ $cm^{-3}$), $V_{OC}$ of the baseline model drops from 825 to 530 mV, while $iV_{OC}$ increases from 835 to 900 mV (shown by solid lines in Figure 5). The $iV_{OC}$–$V_{OC}$ gap increases from 10 to 370 mV with reducing doping. This change in $V_{OC}$ and $iV_{OC}$ corresponds well to the change in measured $V_{OC}$ and $iV_{OC}$ of First Solar As-doped cells with good contacts but gradually reduced doping activation (shown in Figure 4 in Ref. [7], samples 3 → 2 → 1). Therefore, our model of increased $iV_{OC}$ caused by $QFL_p$ bending in the absorber (due to the low partial conductivity of holes) provides a feasible

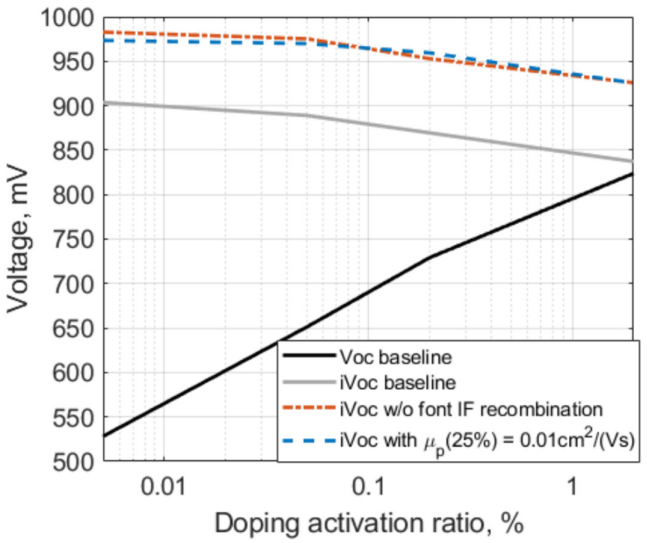


**FIGURE 5** | Calculated dependence of $V_{OC}$ and $iV_{OC}$ on the doping activation ratio using baseline model (Table S3) with total acceptor density of $10^{18}$ $cm^{-3}$ and $\mu_p(25\%) = 0.3$ $cm^2/(V{\cdot}s)$.

explanation of the measured $iV_{OC}$ trend. The $V_{OC}$ loss in the model with reduced doping activation is due to increased recombination in the absorber and at the BI. A similar change in $V_{OC}$ and $iV_{OC}$ can be reproduced using a model with a constant activation ratio and reduced total $As_{Te}$ acceptor density (Figure S5).

We note that the seemingly low hole mobility of 0.3 $cm^2/(V{\cdot}s)$ in $CdSe_{0.25}Te_{0.75}$ does not preclude our model from showing high efficiency when the doping activation ratio is 1% or higher, especially if recombination at the front IF is reduced. This low mobility is in the range of the nanosecond-timescale LITG mobilities measured in Ref. [38], which provides additional support to our baseline model.

The baseline model in Figure 5 does not predict $iV_{OC} > 900$ mV even with a very low doping activation ratio. To understand how an $iV_{OC}$ of 970 mV could be achieved, we analyze how different changes in our baseline device model affect $iV_{OC}$. Changes in the *p*-contact layer properties do not increase $iV_{OC}$. Complete elimination of BI recombination can only increase $iV_{OC}$ to 905 mV. Increasing the absorber lifetime to 1 ms only increases $iV_{OC}$ to 925 mV. The only two changes that bring $iV_{OC}$ to ~970 mV are (i) elimination of FI recombination (no recombination defects at FI) and (ii) reduction of hole mobility to 0.01 $cm^2/(V{\cdot}s)$ in $CdSe_{0.25}Te_{0.75}$ (dot-dashed and dashed lines in Figure 5, respectively). In any case, slow transport of holes and $QFL_p$ inflation in the high-Se region similar to the one shown in Figure 4C is required to achieve an $iV_{OC}$ of 970 mV in our model.

### 3.4 | QFLS and $iV_{OC}$ With Back-Side Illumination

As we show above, a QFLS/q–$V_{OC}$ gap (detected by the $iV_{OC}$–$V_{OC}$ gap) may appear due to various reasons. It is not possible to discriminate between these reasons using front-side measurements alone. Modeling suggests that combining front-side measurements with measurements using illumination from the back side may provide more insight into the cause of the gap. When a transparent back contact is applied on top of the back *p*-contact layer, back-side metrics, such as $V_{OC}$ and $iV_{OC}$, can be extracted. Phillips et al. recently reported an example of employing back-side measurements to extract additional information for diagnosing losses in CdTe cells [43].

When the QFLS/q–$V_{OC}$ gap is caused by $QFL_{n/p}$ bending near a contact, simulations predict an $iV_{OC}$–$V_{OC}$ gap with both front- and back-side illumination (Figure 4D,E). However, illumination from the side opposite to the bad interface leads to a higher $iV_{OC}$–$V_{OC}$ gap because the carrier density is lower near the bad interface (hence, a lower partial carrier conductivity). As a result, the $iV_{OC}$–$V_{OC}$ gap with back-side illumination is higher/lower when QFL bending occurs near the front/back contact.

When the QFLS/q–$V_{OC}$ gap is caused by $QFL_p$ bending inside the absorber and there is no substantial recombination at FI or BI, back-side illumination produces only a minimal $iV_{OC}$–$V_{OC}$ gap corresponding to $iV_{OC}$ inaccuracy in a graded absorber (Figure 4F). Therefore, a significant front-side $iV_{OC}$–$V_{OC}$ gap with a minimal ($\leq 15$ mV) back-side gap suggests $QFL_p$ bending inside the absorber, which is caused by low partial hole conductivity in the high-Se region.

Table 1 summarizes the main features of the analyzed models of high-efficiency graded CdSeTe devices with $10^{16}$-$cm^{-3}$ doping, where the $iV_{OC}$–$V_{OC}$ gap is caused by three different reasons. We note that Table 1 illustrates "pure" scenarios, while in reality, intermediate device operation types may be encountered.

Because the difference between the front- and back-side $iV_{OC}$–$V_{OC}$ gaps is affected by the accuracy of the $iV_{OC}$ metric, it is important to understand how light extraction affects $iV_{OC}$. Simulation results in Figure 4D–F assume perfect PL extraction for both front- and back-side measurements (i.e., complete internal reflection from the interface opposite to the illumination side and no internal reflection from the interface on the illumination side). In practice, however, both front- and back-side $iV_{OC}$ are reduced by a factor $A$ due to imperfect PL extraction, such that $iV_{OC,front} - iV_{OC,back} = kT\log\left(\frac{ERE_{front} \cdot A_{back}}{ERE_{back} \cdot A_{front}}\right)$. The ratio $\frac{A_{back}}{A_{front}}$ must be found for a reference stack of the same type where the front- and back-side $iV_{OC}$–$V_{OC}$ gaps would be the same without PL extraction issues (i.e., an absorber with the same stoichiometry grading but with knowingly high partial conductivities of charge carriers so that QFLS is uniform), and the FI and BI are the same to ensure the same PL internal reflection. The ratio $\frac{A_{back}}{A_{front}}$ should then be used to correct the $iV_{OC,front} - iV_{OC,back}$ difference for an absorber of interest.

## 4 | Discussion

### 4.1 | Physical Meaning of $iV_{OC}$

In simulations, the $iV_{OC}$ change generally follows the QFLS/q change (lower hole mobility yields higher QFLS and $iV_{OC}$). Depending on the model parameters, $iV_{OC}$ can be equal to QFLS/q, or it can be higher or lower than QFLS/q by up to 50 mV. This means that in some cases, the QFLS/q–$V_{OC}$ gap could be even higher than that concluded from the $iV_{OC}$–$V_{OC}$ gap. In addition, this means that, generally, $iV_{OC}$ is not a quantitative

**TABLE 1** | Main features of three categories of models with QFL bending near the FI, the BI, and inside the absorber. Front and back refer to the illumination direction for the $V_{OC}$, $iV_{OC}$ measurements.

| QFL bending | Recombination | Nonuniform QFL | Low mobility | $iV_{OC}$–$V_{OC}$ gap |
|---|---|---|---|---|
| Near FI | At FI | $QFL_n$ | Low $\mu_n$ in high-Se | Front < back |
| Absorber | In absorber | $QFL_p$ | Low $\mu_p$ in high-Se | Back $\leq$ 15 mV |
| Near BI | At BI | $QFL_p$ | Low $\mu_p$ in low-Se | Front > back |

measure of QFLS/q in the absorber. Rather, it could serve as a qualitative indicator of the QFLS/q–$V_{OC}$ gap.

When ERE and $iV_{OC}$ increase due to reduced partial carrier conductivity, $V_{OC}$ does not increase. In this case, an increase in ERE and $iV_{OC}$ is not an indicator of improved absorber quality but quite the opposite: It is a signature of slower transport of photogenerated carriers. With QFL bending near a contact, higher $iV_{OC}$ means slower transport of electrons or holes to the corresponding contact (*n*- or *p*-contact). In the case of $QFL_p$ bending in the absorber bulk, higher $iV_{OC}$ means slower separation of photogenerated carriers at the front and slower majority carriers transport through the absorber to the back.

Only when an $iV_{OC}$ increase is accompanied by a $V_{OC}$ increase can one conclude that recombination is reduced. In this case, however, lower recombination is already indicated by the higher $V_{OC}$ and does not require an additional metric.

## 4.2 | Additional $iV_{OC}$ Errors

In addition to nonuniform $E_g$ and $QFL_{n/p}$, several other factors can affect the accuracy of the $iV_{OC}$ metric and interpretation of an $iV_{OC}$ increase, which we briefly discuss in this section.

### 4.2.1 | Incomplete Reflection From the Back

In our modeling, we assume that all PL emitted backward is fully reflected from the BI and escapes through the front. This assumption may not be fully correct as the BI may reflect only some fraction of light. According to our estimations, if no special measures are taken to ensure full reflection from the back, $iV_{OC}$ may be underestimated by up to ~5 mV in a realistic low-ERE device. This may counteract $iV_{OC}$ inflation due to graded $E_g$, in some cases leading to a very small measured $iV_{OC}$–$V_{OC}$ gap due to cancellation of errors. This becomes especially important when measuring devices with a transparent back contact. The error may be reduced if the amount of PL that escapes through the back can be taken into account when measuring ERE. Similarly, when measuring from the back, PL may partially escape through the front side, which needs to be taken into account.

### 4.2.2 | Errors in $V_{OC,ideal}$

Accurate $iV_{OC}$ calculation relies on the accurate calculation of $V_{OC,ideal}$. In our modeling, the only factor affecting $V_{OC,ideal}$ is the distribution of the radiative recombination rate constant calculated from the absorption spectrum shifted according to $E_g(x)$. In experimental papers, $V_{OC,ideal}$ is calculated using measured absorptance spectrum assuming an absorber with uniform $E_g$. The two possible sources of error here are (i) the assumption of uniform $E_g$, leading to underestimated $V_{OC,ideal}$ for a graded absorber (graded absorber has less radiative recombination in the high-$E_g$ region) and (ii) the accuracy of the absorptance spectrum, which should be measured in a very wide dynamic range to capture the possible contribution of weak tails.

### 4.2.3 | "ERE Derivative" Method

An accurate calculation of ERE requires knowledge of the total photogeneration rate and radiative recombination rate as measured by the photon flux of absolute PL under 1 sun open-circuit conditions [5, 11, 44]. To avoid possible errors when processing absolute PL and to simplify the equipment, Onno et al. [7] proposed an alternative method to calculate ERE. The method measures the change in emitted photon flux with a small additional excitation (< 0.05 sun) under a constant 1 sun bias light. This method essentially provides the ERE derivative with respect to excitation at an excitation of 1 sun, which generally is not the same as 1 sun ERE.

To estimate the $iV_{OC}$ error introduced by the "ERE derivative" method compared to ERE, we implement an "ERE derivative" simulation method into the drift–diffusion solver to reproduce the experimental method in Ref. [7]. We perform a number of $iV_{OC}$ simulations with graded absorbers and different model parameters. We include device models limited by FI, absorber, or BI recombination and vary mobilities in a wide range. By comparing the $iV_{OC}$ values calculated using the ERE and "ERE derivative" methods, we find that $iV_{OC}$ (ERE derivative) exceeds $iV_{OC}$ (ERE) by 5–15 mV. The reason is that the slope of PL (excitation) becomes steeper as the excitation approaches 1 sun, yielding higher "ERE derivative" values compared to ERE. This change of the PL (excitation) slope is due to the different distribution of charge carriers and recombination in the absorber at different excitation levels. We conclude that the "ERE derivative" method leads to $iV_{OC}$ overestimation of 5–15 mV.

### 4.2.4 | Trap-to-Band PL

All the formalism for the $iV_{OC}$ metric is based on the assumption of band-to-band PL only, where the radiative rate is defined by the concentrations of both charge carriers. In the case of trap-to-band radiative transitions, the radiative rate is defined by the product of only one charge carrier density and the empty trap density, and generally, may not be directly proportional to the density of the other charge carrier. In this case, PL and PL-derived metrics ($iV_{OC}$) may not directly correlate with QFLS, introducing an unknown error. Detailed analysis of such scenarios is beyond the scope of this paper.

## 4.3 | Physical Meaning of Selectivity

The most widely used definition of selectivity is the $V_{OC}/iV_{OC}$ ratio extracted from experimental measurements. The selectivity is below 1 when $iV_{OC} > V_{OC}$. Our modeling results suggest that even with perfect contacts, selectivity can be < 1 for a CdSeTe absorber when the partial conductivity of holes in the absorber is low. In cases when selectivity < 1 is caused by near-contact QFL bending, it is a combination of the absorber/contact interface properties (such as band offset and defect density) and partial conductivities of carriers in the absorber that is responsible for low $V_{OC}/iV_{OC}$, rather than the internal properties of a contact layer. Similar conclusions were reached in Ref. [18] using SCAPS simulations of $V_{OC}/(QFLS/q)$ for a uniform CdTe absorber with different absorber and interface properties.

Our results additionally suggest that selectivity < 1 may be a result of absorber grading and the "ERE derivative" method used for $iV_{OC}$ measurement. Depending on the Se profile, absorber thickness, internal reflectance of the back contact, recombination in the cell, and cell $V_{OC}$, selectivity can range from 0.96 to 1.00 even without any QFLS nonuniformities, i.e., without carrier transport issues. Theoretically, selectivity in the range from 0.96 to 1.00 may partially originate from nonuniform QFLS and partially from errors in the method, but it is impossible to deduce the exact reason from $V_{OC}$ and $iV_{OC}$ values alone. Selectivity values below 0.96 indicate issues with carrier separation and extraction leading to the bending of one QFL near a contact or inside the absorber.

We note that "poor selectivity" or "selectivity losses" are generic terms, which mean that carrier transport somewhere in the stack is slow and may imply any of the possible scenarios of QFL nonuniformity in Figure 1. We purposefully avoid using the term selectivity because of its inherent ambiguity. We note, however, that our results and conclusions do not contradict the concepts of "poor selectivity" or "selectivity losses" in any way. On the contrary, our analysis goes one level deeper and reveals the possible types of "poor selectivity" and their causes.

### 4.4 | Interpretation of Experimental Data

There are two main reasons for increased $iV_{OC}$ in graded CdSeTe absorbers, lower nonradiative recombination and worse carrier transport, and it is important not to confuse them when interpreting experimental data. Below, we discuss our results in more detail, answering several practically important questions.

**Is the $iV_{OC}$ metric alone sufficient to draw any conclusions?** The $iV_{OC}$ metric alone does not provide sufficient information to conclude on the reason of $iV_{OC}$ increase. Higher $iV_{OC}$ can be achieved, e.g., by increasing the Se% in a CdSeTe alloy (leading to deeper acceptors and lower $\mu_p$) or by reducing the *p*-doping or doping activation ratio, which will not result in higher device efficiency because of slower hole transport. Similarly, worse n/p conductivity near the n/p contact (e.g., due to accumulated interface acceptors/donors) may "decouple" $iV_{OC}$ from interface recombination, leading to simultaneously higher $iV_{OC}$ and worse carrier extraction at the n/p contact. We argue that the $iV_{OC}$ measurement alone on a finished or unfinished CdSeTe device may be misleading.

**What does the $iV_{OC}$–$V_{OC}$ gap tell us?** While the $iV_{OC}$ metric alone may be misleading, tracking the $iV_{OC}$–$V_{OC}$ gap during cell optimization may be more useful. An increase in both $iV_{OC}$ and $V_{OC}$ indicates reduced nonradiative recombination, while an increase in the $iV_{OC}$–$V_{OC}$ gap without an increase in $V_{OC}$ indicates increased carrier transport issues. However, we suggest disregarding any changes in the $iV_{OC}$–$V_{OC}$ gap if the gap is within ~15 mV because of the inherent $iV_{OC}$ measurement error in a graded CdSeTe absorber (within 30 mV if the "ERE derivative" method is used).

A possible scenario is when during cell optimization, both $V_{OC}$ and $iV_{OC}$–$V_{OC}$ increase, but the $V_{OC}$ increase is smaller than the $iV_{OC}$ increase. It is possible that both the lifetime increased and the mobility decreased in this case. Increasing the Se% in an alloy leads to reduced hole mobility but also to longer lifetimes, based on TRPL and cathodoluminescence measurements [38, 45]. Therefore, it is possible that increasing Se in a graded CdSeTe alloy may lead simultaneously to lower $\mu_p$ and higher $\tau_e$ in the high-Se region. In this case, both $V_{OC}$ and the $iV_{OC}$–$V_{OC}$ gap may increase. If the $iV_{OC}$–$V_{OC}$ gap becomes noticeably higher than 15 mV, this suggests slower hole transport. If FF is reduced, this is an additional indication of slow hole transport, because slow majority carrier collection (due to low partial conductivity) is one of the major contributors to FF reduction [23].

We note that the same explanation applies when the $iV_{OC}$–$V_{OC}$ gap increases, but $V_{OC}$ does not increase, while the $E_g$–$V_{OC}$ gap reduces instead (due to lower $E_g$). In this case, a decrease in the $E_g$–$V_{OC}$ gap indicates a decrease in nonradiative recombination, while an increase in $iV_{OC}$–$V_{OC}$ gap greater than 15 mV indicates worse carrier transport.

If ERE is measured, but $iV_{OC}$ is not calculated, one may use a simple rule: for each 2× ERE increase, the $E_g$–$V_{OC}$ gap at 300 K should decrease by $kT{\cdot}\log(2) \approx 18$ mV. If the $E_g$–$V_{OC}$ gap reduces significantly by less than 18 mV for a 2× ERE increase, one has to suspect carrier transport issues (or brighter PL from states not contributing to QFLS, such as radiative defects and tail states, which can be determined based on the PL spectrum shape).

**How do back-side measurements improve understanding of the $iV_{OC}$–$V_{OC}$ gap?** Measuring the $iV_{OC}$–$V_{OC}$ gap with front-side illumination alone can detect an $iV_{OC}$–$V_{OC}$ gap change, but it cannot discriminate between the different QFL nonuniformity scenarios that cause the gap. By comparing the $iV_{OC}$–$V_{OC}$ gap from front- and back-side illumination, it may be possible to detect $QFL_p$ nonuniformity inside the absorber, which is caused by slow hole transport through the absorber. In this case, the $iV_{OC}$–$V_{OC}$ gap with back-side illumination should be minimal (corresponding to the $iV_{OC}$ measurement error in a graded absorber).

When the $iV_{OC}$–$V_{OC}$ gap is caused by low QFLS near a contact, comparing the $iV_{OC}$–$V_{OC}$ gap from the two illumination directions could indicate the responsible interface (Section 3.4). However, the actual difference in the $iV_{OC}$–$V_{OC}$ gap with illumination direction depends on various device parameters and, in some cases, may be too small to be reliably detected from the measurements.

**What does the record high $iV_{OC}$ of 970 mV mean?** The low CV doping (~$1–2{\cdot}10^{15}$ $cm^{-3}$) and low doping activation ratio (<< 1%) reported for the high $iV_{OC}$ cell suggest reduced partial conductivity of holes. In our simulations, reduced partial conductivity of holes leads to QFLS inflation in the high-Se region, resulting in an increased $iV_{OC}$ metric without increasing absorber lifetime. A very high value of 970 mV can be simulated using certain combinations of low hole mobility in the high-Se region and recombination at the FI (e.g., $\mu_p(25\%) = 0.01$ $cm^2/(V{\cdot}s)$ and FI defect density of $6{\cdot}10^{10}$ $cm^{-2}$ or $\mu_p(25\%) = 0.3$ $cm^2/(V{\cdot}s)$ and no FI defects). We note that neither an increase in absorber lifetime nor a change in back contact or BI properties allows our model to reproduce an $iV_{OC}$ of 970 mV. At the same time, a very low $V_{OC}$ value (~200 mV) simultaneously with a high-$iV_{OC}$

of 970 mV (as reported in Ref. [7]) cannot be achieved by simply changing hole mobility and FI properties. Additional $QFL_p$ bending inside a highly resistive back contact layer (illustrated in Figure 1D) could explain a very low $V_{OC}$. Simulation of such bending using a model with a graded absorber, low compensated doping, and low hole mobility is computationally challenging and is out of the scope of this paper.

**Does higher PL mean higher efficiency?** Generally, the forward statement is valid: high efficiency leads to high PL (hence high ERE and high $iV_{OC}$) because the nonradiative recombination is lower in high-efficiency cells. However, the reverse statement—high PL leads to high efficiency—is not necessarily true. Our simulations show that carrier transport issues may simultaneously lead to higher PL but lower photoconversion efficiency.

It is correct to say that a cell with low ERE or low PL will not reach record efficiency values. This is why there is a correlation between the $E_g$–$V_{oc}$ gap and ERE for high-performance cell [3, 4]. Achieving high PL (or $iV_{OC}$) by means of achieving high $V_{OC}$ is a logically correct and practically important goal. However, achieving high PL (or $iV_{OC}$) by any means is not a correct goal because this does not guarantee higher efficiency or better absorber quality.

## 5 | Conclusions

Through detailed numerical analysis, we consider the complex interplay between the carrier separation and recombination dynamics in a realistic graded CdSeTe absorber with low hole mobility and bandgap grading. Our results indicate that $iV_{OC}$ measurements alone can result in misleading conclusions about the absorber quality and device operation.

Specifically, we demonstrate the following:

1. A reason for $QFLS/q > V_{OC}$ is slow transport of charge carriers, which is not beneficial to PV device performance.
2. In a realistic graded CdSeTe absorber, $iV_{OC}$ is not a direct measure of QFLS/q in the absorber. $iV_{OC}$ generally follows the maximum QFLS/q but may be higher or lower by up to 50 mV.
3. The $iV_{OC}$ metric alone may be misleading. The increased $iV_{OC}$ of a graded CdSeTe absorber may indicate QFLS inflation in the high-Se region due to slow hole transport rather than reduced recombination.
4. The experimentally reported increase in the $iV_{OC}$–$V_{OC}$ gap of 360 mV with reduced doping can be reproduced using a model with sub-1 $cm^2/(V{\cdot}s)$ hole mobility in the high-Se region.
5. To determine the reason for the $iV_{OC}$–$V_{OC}$ gap, one can compare $iV_{OC}$–$V_{OC}$ gaps when the device is illuminated from different sides. A large front-side $iV_{OC}$–$V_{OC}$ gap but a very low back-side $iV_{OC}$–$V_{OC}$ gap indicates slow hole transport in the high-Se region near the front side with recombination mostly in absorber. When an $iV_{OC}$–$V_{OC}$ gap is present with both front- and back-side illumination, a larger gap from front-(back-)side illumination indicates QFLS loss near the back (front) due to a recombinative back (front) IF and low partial conductivity of holes (electrons) near the corresponding contact.
6. High efficiency leads to high PL and ERE. However, the reverse statement is not always true when realistic carrier mobilities are considered. The goal of achieving high $iV_{OC}$ (or PL or ERE) by any means is not a correct goal. Absorber optimization toward high PL may result in an absorber with lower lifetime and lower carrier conductivity.

Unfortunately, the complex properties of thin-film CdSeTe cells make the utilization and interpretation of indirect experimental metrics considerably more challenging. Sometimes, $iV_{OC}$ is referred to as a simple and straightforward metric that characterizes a solar cell under practically relevant 1 sun open-circuit conditions as opposed to, e.g., TRPL. In reality, however, a comprehensive model of the $iV_{OC}$ measurement, based on a realistic solar cell device model, is required for correct interpretation. This is generally also true for many other indirect measurements.


### Acknowledgments

We thank Carey Reich and Jialiu Ma for fruitful discussions.


### Data Availability Statement

The data that support the findings of this study are available from the corresponding author upon reasonable request.

### References


1. https://www.nrel.gov/pv/cell-efficiency.html, accessed September 9th, 2024.

2. O. D. Miller, E. Yablonovitch, and S. R. Kurtz, "Strong Internal and External Luminescence as Solar Cells Approach the Shockley–Queisser Limit," *IEEE Journal of Photovoltaics* 2 (2012): 303–311.

3. M. A. Green and A. W. Y. Ho-Baillie, "Pushing to the Limit: Radiative Efficiencies of Recent Mainstream and Emerging Solar Cells," *ACS Energy Letters* 4, no. 7 (2019): 1639–1644.

4. M. Yamaguchi, K.-H. Lee, K. Araki, N. Kojima, H. Yamada, and Y. Katsumata, "Analysis for Efficiency Potential of High-Efficiency and Next-Generation Solar Cells," *Progress in Photovoltaics: Research and Applications* 26, no. 8 (2018): 543–552.

5. P. Wurfel, "The Chemical Potential of Radiation," *Journal of Physics C: Solid State Physics* 15 (1982): 3967–3985.

6. T. Kirchartz and U. Rau, "What Makes a Good Solar Cell?," *Advanced Energy Materials* 8 (2018): 1703385.

7. A. Onno, C. Reich, S. Li, et al., "Understanding What Limits the Voltage of Polycrystalline CdSeTe Solar Cells," *Nature Energy* 7 (2022): 400–408.

8. T. Kirchartz, J. A. Márquez, M. Stolterfoht, and T. Unold, "Photoluminescence-Based Characterization of Halide Perovskites for Photovoltaics," *Advanced Energy Materials* 10, no. 26 (2020): 1904134.

9. S. Siebentritt, T. P. Weiss, M. Sood, M. H. Wolter, A. Lomuscio, and O. Ramirez, "How Photoluminescence Can Predict the Efficiency of Solar Cells," *Journal of Physics: Materials* 4 (2021): 042010.

10. P. Caprioglio, M. Stolterfoht, C. M. Wolff, et al., "On the Relation Between the Open-Circuit Voltage and Quasi-Fermi Level Splitting in

Efficient Perovskite Solar Cells," *Advanced Energy Materials* 9 (2019): 1901631.

11. C. Dreessen, K. P. S. Zanoni, L. Gil-Escrig, et al., "When JV Curves Conceal Material Improvements: The Relevance of Photoluminescence Measurements in the Optimization of Perovskite Solar Cells," *Advanced Optical Materials* 12 (2024): 2301019.

12. F. Babbe, L. Choubrac, and S. Siebentritt, "The Optical Diode Ideality Factor Enables Fast Screening of Semiconductors for Solar Cells," *Solar RRL* 2 (2018): 1800248.

13. N. P. Irvin, S. J. Babcock, E. Y. Chen, R. R. King, and C. B. Honsberg, "Feedback Between Radiation and Transport in Photovoltaics," *Progress in Photovoltaics: Research and Applications* 31 (2023): 283–301.

14. K. Toprasertpong, A. Delamarre, Y. Nakano, J.-F. Guillemoles, and M. Sugiyama, "Generalized Reciprocity Relations in Solar Cells With Voltage-Dependent Carrier Collection: Application to P-I-N Junction Devices," *Physical Review Applied* 11 (2019): 024029.

15. C. Reich, *Investigations to Improve CdTe Based Solar Cell Open Circuit Voltage and Efficiency Using Passivation and Selectivity Theoretical Framework*, Ph. D. Thesis, (Colorado State University, 2022).

16. A. Onno, C. Chen, P. Koswatta, M. Boccard, and Z. C. Holman, "Passivation, Conductivity, and Selectivity in Solar Cell Contacts: Concepts and Simulations Based on a Unified Partial-Resistances Framework," *Journal of Applied Physics* 126 (2019): 183103.

17. J. Warby, S. Shah, J. Thiesbrummel, et al., "Mismatch of Quasi–Fermi Level Splitting and $V_{OC}$ in Perovskite Solar Cells," *Advanced Energy Materials* 13, no. 2023 (2023): 2303135.

18. J. Friedl, *Understanding CdSeTe/CdTe Photovoltaic Materials and Devices Through Advanced Numerical Simulation and Optoelectronic Characterization*, Ph. D. Thesis, (University of Toledo, 2024).

19. R. Mallick, X. Li, C. Reich, et al., "Arsenic-Doped CdSeTe Solar Cells Achieve World Record 22.3% Efficiency," *IEEE Journal of Photovoltaics* 13, no. 2023 (2023): 510–515.

20. I. Turkevych, R. Grill, J. Franc, E. Belas, P. Hoschl, and P. Moravec, "High-Temperature Electron and Hole Mobility in CdTe," *Semiconductor Science and Technology* 17 (2002): 1064–1066.

21. K. Alberi, O. D. Dubon, W. Walukiewicz, K. M. Yu, J. A. Gupta, and J.-M. Baribeau, "Composition Dependence of Hole Mobility in $GaSb_xAs_{1-x}$," *Applied Physics Letters* 92 (2008): 162105.

22. L. Hsu, R. E. Jones, S. X. Li, K. M. Yu, and W. Walukiewicz, "Electron Mobility in InN and II-N Alloys," *Journal of Applied Physics* 102 (2007): 073705.

23. U. Wurfel, A. Cuevas, and P. Wurfel, "Charge Carrier Separation in Solar Cells," *IEEE Journal of Photovoltaics* 5 (2015): 461–469.

24. K. K. Chin, "P-Doping Limit and Donor Compensation in CdTe Polycrystalline Thin Film Solar Cells," *Solar Energy Materials & Solar Cells* 94 (2010): 1627–1629.

25. M. Forster, F. E. Rougieux, A. Cuevas, et al., "Incomplete Ionization and Carrier Mobility in Compensated p-Type and n-Type Silicon," *IEEE Journal of Photovoltaics* 3, no. 1 (2013): 108–113.

26. I. Sankin and D. Krasikov, "Kinetic Simulations of Cu Doping in Chlorinated CdSeTe PV Absorbers," *Physica Status Solidi A: Applications and Materials Science* 216 (2019): 1800887.

27. M. H. Rahman, S. Rojsatien, D. Krasikov, M. Bertoni, M. K. Y. Chan, A. Mannodi-Kanakkithodi, *First Principles Investigation of Dopants and Defect Complexes in CdSexTe1−x*, in preparation.

28. S. A. Jensen, J. M. Burst, J. N. Duenow, et al., "Long Carrier Lifetimes in Large-Grain Polycrystalline CdTe Without CdCl2," *Applied Physics Letters* 108 (2016): 263903.

29. A. Zunger, "Practical Doping Principles," *Applied Physics Letters* 83 (2003): 57–59.

30. M. Lingg, A. Spescha, S. G. Haass, R. Carron, S. Buecheler, and A. N. Tiwari, "Structural and Electronic Properties of CdTe1-xSexfilms and Their Application in Solar Cells," *Science and Technology of Advanced Materials* 19 (2018): 683–692.

31. X. Xiang, Y. Tong, A. Gehrke, and S. T. Dunham, "Point Defects in CdTe and CdTeSe Alloy: A First Principles Investigation With DFT+U," *Physical Review Materials* 8 (2024): 084602.

32. K. Decock, *Defect Related Phenomena in Chalcopyrite Based Solar Cells*, PhD Thesis (Ghent University, Department of Electronics and information systems, 2012).

33. A. R. Shaik, D. Brinkman, I. Sankin, et al., "PVRD-FASP: A Unified Solver for Modeling Carrier and Defect Transport in Photovoltaic Devices," *IEEE Journal of Photovoltaics* 9, no. 6 (2019): 1602–1613.

34. P. Wurfel and U. Wurfel, *Physics of Solar Cells*, 3rd ed. (Willey-VCH, 2016).

35. M. Burgelman, P. Nollet, and S. Degrave, "Modelling Polycrystalline Semiconductor Solar Cells," *Thin Solid Films* 361–362 (2000): 527–532.

36. D. Krasikov and I. Sankin, "Beyond Thermodynamic Defect Models: A Kinetic Simulation of Arsenic Activation in CdTe," *Physical Review Materials* 2 (2018): 103803.

37. P. Ščajev, M. Nardone, C. Reich, et al., "Kuciauskas As-Doped Polycrystalline CdSeTe: Localized Defects, Carrier Mobility and Lifetimes, and Impact on High-Efficiency Solar Cells," *Advanced Energy Materials* 15 (2024): 2403902.

38. J. Yang and S. H. Wei, "First-Principles Study of the Band Gap Tuning and Doping Control in CdSe*x*Te1−*x* Alloy for High Efficiency Solar Cell," *Chinese Physics B* 28 (2019): 086106.

39. T. Song, A. Kanevce, and J. R. Sites, "Emitter/Absorber Interface of CdTe Solar Cells," *Journal of Applied Physics* 119 (2016): 233104.

40. A. Sharan, M. Nardone, D. Krasikov, N. Singh, and S. Lany, "Atomically Thin Interlayer Phase From First Principles Enables Defect-Free Incommensurate SnO2/CdTe Interface," *Applied Physics Reviews* 9 (2022): 041411.

41. P. Gorai, D. Krasikov, S. Grover, G. Xiong, W. K. Metzger, and V. Stevanović, "A Search for New Back Contacts for CdTe Solar Cells," *Science Advances* 9 (2023): eade3761.

42. R. T. Tung and L. Kronik, "Band Offset Formation at Semiconductor Heterojunctions Through Density-Based Minimization of Interface Energy," *Physical Review B* 94, no. 2016 (2016): 075310.

43. A. B. Phillips, J. D. Friedl, K. K. Subedi, et al., "Approach to Determining the Limiting Recombination Mechanism in CdTe-Based Solar Cells," *Solar Energy Materials and Solar Cells* 266 (2014): 112689.

44. D. Kuciauskas, J. Moseley, P. Ščajev, and D. Albin, "Radiative Efficiency and Charge-Carrier Lifetimes and Diffusion Length in Polycrystalline CdSeTe Heterostructures," *Physica Status Solidi RRL: Rapid Research Letters* 14, no. 3 (2020): 1900606.

45. T. A. M. Fiducia, B. G. Mendis, K. Li, et al., "Understanding the Role of Selenium in Defect Passivation for Highly Efficient Selenium-Alloyed Cadmium Telluride Solar Cells," *Nature Energy* 4 (2019): 504–511.

## Supporting Information

Additional supporting information can be found online in the Supporting Information section.